GENIORS

Research and Innovation Action (RIA)

This project has received funding from the European Union's Horizon 2020 research and innovation programme under grant agreement No 755171.

Start date : 2017-06-01 Duration : 48 Months
http://geniors.eu/

Performances on microelectrode for online monitoring of relevant parameters

Authors : Pr. Mount ANDY (UEDIN), Ilka Schmueser

GENIORS - Contract Number: 755171

Project officer: Roger Garbil

Document title	Performances on microelectrode for online monitoring of relevant parameters
Author(s)	Pr. Mount ANDY, Ilka Schmueser
Number of pages	27
Document type	Deliverable
Work Package	WP5
Document number	D5.3
Issued by	UEDIN
Date of completion	2019-07-05 14:43:24
Dissemination level	Public

Summary

The results presented in this deliverable report together indicate that we have developed electrochemical microelectrode array sensor systems which are capable of electrochemical measurements rich in diagnostic information, specifically enabling quantitative electrochemical analysis in the harsh environment presented by the acid systems required for EURO-GANEX liquid-liquid extraction, and which are unaffected by initial irradiation tests. The enhanced electrochemical pulse technique of Differential Pulse Voltammetry, has shown superior performance in terms of enhanced sensitivity, decreased background and increased signal-to-noise compared to the more commonly used cyclic voltammetry. Nafion has also been shown to be an effective, acid stable, protective and selectively permeable polymer membrane for the protection of the platinum from corrosive ion formation such as CeIV. It is also capable of screening out large ions and/or molecules due to its characteristic pore size in the range of single nanometres. This opens up the prospect of selective detection of free cations without detection of bulky iron complexes. The backbone anions of these pores additionally make it potentially able to favour cation (FeIII) aggregation through selective binding. In terms of quantitative detection, analysis of the DPV response on bare platinum arrays has indicated quantitative electrochemical reduction peaks characteristic of nitrite, a 1:1 FeIII-ligand complex and total FeIII for the exemplar FeIII and ligand (SO3-Ph-BTBP) system. These measurements are consistent with benchmark fluorescence measurements but richer in information, in providing independent measurement of total FeIII present in solution, complexed FeIII and nitrite concentration. That the SO3-Ph-BTBP:FeII complex apparently undergoes a further one electron electrochemical reduction (most likely involving mixed metal ligand orbitals) potentially opens up the possibility of detecting other metal ions that do not undergo an electrochemical redox reaction when uncomplexed, either through a similar complex reduction or through the addition of conjugated redox active groups to the ligand to report on metal complexation. When combined with the established microelectrode array characteristics of enhanced detection sensitivity, lower susceptibility to convection and lower limits of detection, these proof of principle results demonstrate the potential of these systems for process characterisation and for sensing and...

Approval

Date	By
2019-07-06 21:46:03	Pr. Christian EKBERG (Chalmers)
2019-09-17 13:28:51	Dr. Jean-Marc ADNET (CEA)
2019-11-05 09:25:28	Mr. Stéphane BOURG (CEA)

CONTENT

This project has received funding from the EURATOM research and training programme 2014-2018 under grant agreement No 755171. The content of this deliverable reflects only the author's view. The European Commission is not responsible for any use that may be made of the information it contains.

INTRODUCTION

Understanding, controlling and monitoring the solvent extraction process, which forms part of the EURO-GANEX process, requires precise knowledge of processing parameters such as the solvent and extractant quality and the local concentrations of various analytes, including selected metal ions and NO_x species. Electrochemical sensors are one of the potential methods to be investigated for the on-line monitoring of the process, alongside optical techniques such as UV/vis spectroscopy.

Previous work on the development of miniaturised electrochemical sensors in the predecessor program SACSESS has shown the capabilities of these sensors for quantitative sensing of nitric acid derived products and redox couples. This work is now expanded on during GENIORS to investigate the further potential for the monitoring of the extraction of metal ions.

Electrochemical sensors have several advantages over optical systems in that they do not require optical windows in the equipment or sensitive/expensive optical instrumentation and can measure local and bulk concentrations in in highly scattering or absorbing solutions (e.g. those containing particulates, droplets or opaque solutions). In many cases simple systems and instrumentation can be used for quantitative in-situ sensing of electroactive species, and the relative contributions of concentration (thermodynamics) and mass transport through convection and/or diffusion (kinetics) can be extracted. Overall, electrochemical sensors can produce signals from an analyte provided it is present in the sensor's immediate vicinity, and undergoes or specifically perturbs an electrochemical reaction under the relevant conditions.

The sensors being investigated in this work use miniature platinum microelectrodes fabricated using semi-conductor manufacturing techniques on silicon substrates. The required sensitivity and typical analyte concentration ranges required for the extraction monitoring make these types of electrodes ideally suited to this application due to their high signal-to-noise ratio, low limit of detection, low voltage drop and low susceptibility to convection. The extreme acidic conditions necessitate a robust sensor design and construction, which we have previously validated in proof of principle experiments. The low susceptibility to natural convection (which suggest low susceptibility to forced convection and to the presence of particulates and liquid droplets) is particularly attractive in this application, with its requirement for dynamic mixing to enhance the rate of extraction. Further to the development of microelectrodes, the potential for use of surface modifying electrode layers is investigated, to allow for the protection of the electrode from fouling in these complex analyte mixtures as well as selective screening of analytes, by e.g. their size and/or charge, thereby controlling the measurement selectivity.

This project has received funding from the EURATOM research and training programme 2014-2018 under grant agreement No 755171. The content of this deliverable reflects only the author's view. The European Commission is not responsible for any use that may be made of the information it contains.

THEORY AND BACKGROUND

The sensors used in this study utilise amperometric detection, by which an applied potential to the working electrode with respect to a reference electrode causes an electrochemical redox reaction at the electrode surface and the resultant current flow is measured. In this application these redox reactions can be due to species arising from the solvent, due to solvated metal species and/or due to electroactive extraction ligands.

Nitric acid, used as the aqueous extraction solvent at concentrations up to about 4 M, contains several electrochemically active species. The most important of the electrochemical reactions of nitrate occurring within the electrochemical solvent window, defined by H_2 and O_2 evolution, (at pH 0, the standard condition) are listed in Table 1.

Table 1 Thermodynamics of selected electrochemical reactions of nitric acid under standard conditions[1].

	Reaction			E [V]	Comments
1	$2H_3O^+ + 2e^-$	→	$H_2 + 2H_2O$	0	H_2 evolution reduction solvent limit
2	$NO_3^- + 2H_3O^+ + e^-$	→	$½N_2O_4 + 3H_2O$	0.803	
3	$NO_3^- + 9H_3O^+ + 8e^-$	→	$NH_3 + 12H_2O$	0.81	
4	$NO_3^- + 2H_3O^+ + e^-$	→	$NO_2 + 3H_2O$	0.835	
5	$NO_3^- + 3H_3O^+ + 2e^-$	→	$HNO_2 + 4H_2O$	0.94	
6	$NO_3^- + 4H_3O^+ + 3e^-$	→	$NO + 6H_2O$	0.957	
7	$6H_2O$	→	$4H_3O^+ + O_2 + 4e^-$	1.229	O_2 evolution oxidation solvent limit

It must be remembered that although thermodynamically favoured these reactions are kinetically hindered (as evidenced by the fact that significant peaks are not observed for these processes at a platinum electrode in pure nitric acid solutions at concentrations up to 3 M, despite the fact that nitrate is present in large concentration). However, with time and/or in the presence of redox agents and/or catalysts some of these species are likely to form. Indeed our previous work has detected such species, attributing the observed response to the reduction and oxidation of NO^+/NO_2^-. [2]

1 Mishra et al., Electrochimica Acta, 160 (2015) 219-226

[2] C. L. Brady *'The development and Characterisation of Microelectrodes for Extreme Environments'* PhD thesis, University of Edinburgh, 2013

This project has received funding from the EURATOM research and training programme 2014-2018 under grant agreement No 755171. The content of this deliverable reflects only the author's view. The European Commission is not responsible for any use that may be made of the information it contains.

In addition to these reactions, the analytes to be expected in the process were extracted from OECD NEA Spent Nuclear Fuel Assay Data for Isotopic Validation.[3] Typical corrosion products (e.g. those metal ions resulting from elements such as Fe and Cr in steel, which is a likely material for the piping and vessels) were also considered.[4] For each element, the thermodynamically favoured electrochemical reactions within the solvent window of water for a pH between -0.5 and 1, equivalent to acid concentrations of between around 3 M and 0.1 M HNO_3, were considered. The precise redox potential observed for each reaction of course not only depends on the pH for those where H_3O^+ ions are involved in the redox reaction, but also on the dissolved activities (concentrations) of the oxidised and reduced species, so to capture all possible reactions here, the soluble analyte concentrations were varied between practical concentration limits of 10 nM and 10 M. Table 2 presents a summary of these data. It again needs to be noted that these are thermodynamic calculations, which do not consider kinetic effects.

3 Spent Nuclear Fuel Assay Data for Isotopic Validation OECD NEA, NEA/NSC/WPNCS/DOC(2011)5, 2011, Tables 1, 3, 4

4 Pourbaix diagrams generated through https://materialsproject.org/, and references Kim & Osseo-Assare, Hydrometallurgy 113-114 (2012) 67-78, Hixon & Powell, Environmental Science: Processes & Impacts, 20 (2018) 1306-1322, Cota-Sanchez et al., CNL Nuclear Review, 7(2) (2018) 165-175, Altmaier & Vercouter, Aquatic chemistry of the actinides: aspects relevant to their environmental behaviour in Radionuclide Behaviour in the Natural Environment - Science, Implications and Lessons for the Nuclear Industry, Woodhead Publishing Series in Energy (2012) 44-69, Piro et al., Proceedings of the 11th International Conference on CANDU Fuel (2010), Brookings Eh-pH Diagrams for Geoelectrochemistry, Springer Verlag (1988)

This project has received funding from the EURATOM research and training programme 2014-2018 under grant agreement No 755171. The content of this deliverable reflects only the author's view. The European Commission is not responsible for any use that may be made of the information it contains.

Table 2 Relevant elements and their electrochemical reactions in the solvent window of nitric acid between pH 1 and pH -0.5. All reactions that can thermodynamically occur are listed, including reactions that are only possible at certain analyte concentrations and pressures.

Element	Reaction
Ac	No data found
Ag	$Ag^{+}(aq)/Ag(s)$
Am	/
C	/
Ca	/
Cd	/
Ce	$Ce^{3+}(aq)/CeO_2(s)$
Cl	$Cl^{-}(aq)/ClO_2\,(g)$
Cm	/
Cr	/
Cs	/
Dy	/
Er	/
Eu	/
Fe	$Fe^{3+}(aq)/Fe^{2+}(aq)$
Gd	/
Ho	/
I	$I^{-}(aq)/I^{3-}(aq)$
La	/
Lu	/
Mo	$Mo^{3+}(aq)/MoO_2(s)$
Nb	/
Nd	/
Ni	$Ni^{2+}(aq)/Ni(s)$
Np	$NpO_2^{+}(aq)/NpO_2^{2+}(aq)$
	$NpO_2^{+}(aq)/Np(OH)_2^{2+}(aq)$
	$Np^{3+}(aq)/Np(OH)_2^{2+}(aq)$
	$Np^{3+}(aq)/Np^{4+}(aq)$
	$Np^{4+}(aq)/NpO_2^{+}(aq)$
	$Np^{3+}(aq)/NpO_2(s)$
	$NpO_2^{+}(aq)/NpO_2(s)$
Pa	No data found
Pb	/
Pd	$Pd^{2+}(aq)/Pd(s)$
	$Pd^{2+}(aq)/PdO_2$
Pm	No data found

Element	Reaction
Pr	/
Pu	$PuO_2^{2+}(aq)/PuO_2^{+}(aq)$
	$Pu^{3+}(aq)/Pu^{4+}(aq)$
	$Pu^{4+}(aq)/PuO_2^{2+}(aq)$
	$PuO_2^{2+}(aq)/Pu(OH)_2^{2+}(aq)$
	$PuO_2^{+}(aq)/Pu^{3+}(aq)$
	$Pu^{3+}(aq)/\ Pu(OH)_2^{2+}(aq)$
	$Pu^{3+}(aq)/PuO_2(s)$
	$Pu^{4+}(aq)/PuO_2(s)$
Ra	/
Re	$Re^{+}(aq)/ReO_3(s)$
	$ReO_4^{-}(aq)/ReO_3(s)$
	$Re^{+}(aq)/ReO_4^{-}(aq)$
Rh	$Rh^{2+}(aq)/RhO_2(s)$
	$Rh^{2+}(aq)/Rh(s)$
Ru	$Ru(OH)_2^{2+}(aq)/Ru(s)$
	$Ru(OH)_2^{2+}(aq)/RuO_4(s)$
Sb	$SbO^{+}(aq)/SbO_2(s)$
Se	$H_2Se(aq)/Se(s)$
Sm	/
Sn	$Sn^{2+}(aq)/Sn^{4+}(aq)$
	$Sn^{2+}(aq)/SnO(OH)^{+}(aq)$
	$Sn^{2+}(aq)/SnO_2(s)$
Sr	/
Tb	/
Tc	$Tc^{2+}(aq)/TcO_2(s)$
Te	$Te(OH)^{3+}(aq)/H_2TeO_4(s)$
	$Te^{4+}(aq)/H_2TeO_4(s)$
	$Te^{4+}(aq)/Te(s)$
	$Te(OH)^{3+}(aq)/Te(s)$
	$Te(s)/H_2Te(aq)$
Th	/
Tm	/
U	$UOH^{3+}(aq)/UO_2^{2+}(aq)$
Yb	/
Zr	/

Although, in addition to the nitric acid species and the analytes presented in Table 2, the extraction ligands will also be present in the measurement solution, it is worth noting that no

This project has received funding from the EURATOM research and training programme 2014-2018 under grant agreement No 755171. The content of this deliverable reflects only the author's view. The European Commission is not responsible for any use that may be made of the information it contains.

directly relevant literature information was available on the electrochemical signatures of likely extraction ligands. This collected information informs both this initial study and the further development and assessment of the potential application of these amperometric electrochemical sensors.

ENGINEERING DESIGN AND FABRICATION

DESIGN OF THE ELECTROCHEMICAL TEST STATION AND CONNECTIONS

The development work done under the SACSESS program has highlighted the practical importance of packaging, connections and ventilation in the experimental design. The fumes created by these strongly acidic solutions led to significant corrosion of connections to the chip substrates and the use of a Faraday cage to remove noise and enhance detection sensitivity introduced delays and reduced throughput through complicating adjustments to the setup. As part of GENIORS, the test bed detailed in Figure 1 has therefore been designed to mitigate these issues.

In contrast to typically used setups for electrochemical measurements with microelectrodes, this setup allows the testing of concentrated acid samples and organic solvents, as well as enabling sparging and the extraction of corrosive and/or toxic fumes that may be generated (electro-)chemically. The adaptations to achieve this were (Figure 1):

- A chemically resistant Faraday cage with spill catch
- Stainless steel clamps and stands
- Use of thick wall (~3 mm) and base (~3 cm) glassware with small sample volumes of typically less than 3 ml
- Fabrication of lids for glassware with inlets for electrodes and gases to enable measurements in an oxygen free environment
- Installation of a driven argon inlet line to and exhaust from the Faraday cage
- Fabrication of gold coated corrosion-resistant sample holders for working and counter electrodes with double shielded cables for connection to potentiostat instrumentation outside the Faraday cage.

These measures ensured that long-time measurements could be carried out without the danger of corrosion of the equipment, which has in the past limited the duration of experiments, particularly when using aqueous acids at concentrations above 1 M.

This project has received funding from the EURATOM research and training programme 2014-2018 under grant agreement No 755171. The content of this deliverable reflects only the author's view. The European Commission is not responsible for any use that may be made of the information it contains.

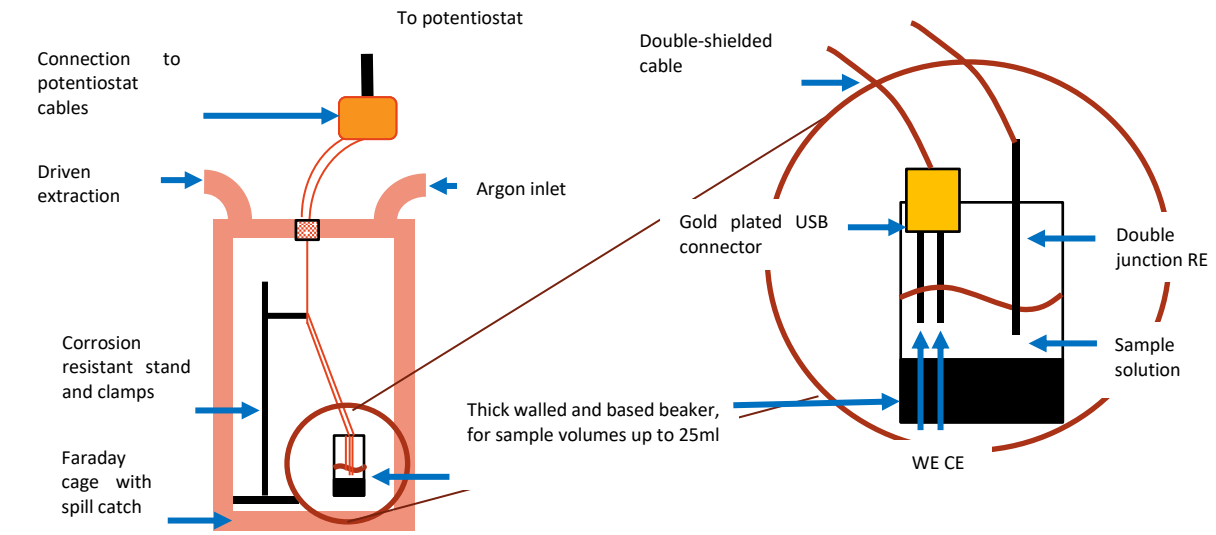

Figure 1 Schematic of measurement setup used for millilitre scale experiments

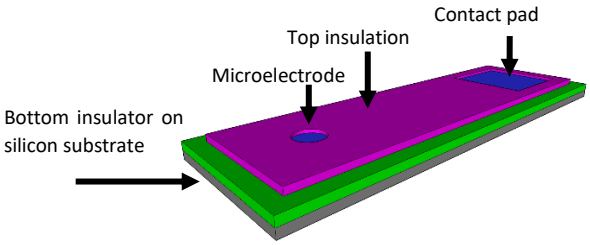

Figure 2 Sketch showing the structure of the platinum microelectrode electrode devices.

CHOICE OF ELECTRODES

Previous work within the SACSESS project has established the capabilities of simple platinum recessed microdisc working electrodes for quantitative sensing in nitric acid; a sketch of the typical design is shown in Figure 2. These electrodes were chosen because they offer the advantages of miniaturised electrodes such as low limit of detection, susceptibility to convection, high signal-to-noise ratio and a time-independent and analytically established steady-state current response as well as ready and high fidelity microfabrication. While this electrode miniaturisation brings these advantages, it also results in low overall currents, which previously required the use of a Faraday cage for measurements of low concentration analytes with sufficient signal-to-noise.

In some measurements, Faraday cage screening is impractical and/or detection limits need to be enhanced further. To address this, as part of this programme, the use of arrayed microdisc electrodes was investigated. Under defined measurement conditions where the electrodes operate independently and their individual signals are combined, these offer the same advantages as these single microdisc electrodes, while also multiplying the observed currents by the number of individual electrodes within the array. This amplifies the redox current into

This project has received funding from the EURATOM research and training programme 2014-2018 under grant agreement No 755171. The content of this deliverable reflects only the author's view. The European Commission is not responsible for any use that may be made of the information it contains.

readily measurable ranges and therefore allows data collection for systems at low concentration (low signal) and/or with high noise that are otherwise difficult to measure.

Our previous work in SACSESS shows the potential for measuring acid using clean bare Pt electrodes in pure aqueous nitrate. However, the issue with such electrodes is their potential to suffer from adsorption of other redox active and inactive species in complex mixtures, which will affect the fidelity and longevity of the response. Therefore we have explored the potential for the use of surface modification by porous polymer films which should reduce or remove such effects by introducing molecular sieving. The chosen film for this proof-of-principle study was Nafion, which can be deposited using standard microfabrication techniques and is a porous polymeric film known to be stable to strong aqueous acidic solutions. Its pores typically are of the order of a few nanometres in diameter, comparable with the dimension of larger uncomplexed and/or complexed metal ions, thereby conferring sieving properties through ion size. It also possesses a relatively high concentration of fixed polymer backbone anion (negatively charged) sites. This therefore offers the further potential for sieving through ion charge induced Donnan membrane potential effects (anion exclusion and cation inclusion) and/or selectivity through specific multivalent cation binding to multiple backbone anions.

MICROFABRICATION

A range of platinum electrodes has been fabricated over the course of the GENIORS project, all based on variations of semiconductor manufacturing processes. All are based on a thin layer of platinum sandwiched between two insulation layers on a silicon substrate with openings in the insulation to expose the metal (Figure 2).

First, a 500 nm to 1000 nm silicon dioxide layer was thermally grown on a silicon wafer forming the bottom insulator between the electrode metal and the silicon, followed by the deposition of an adhesion layer of 10 nm titanium and the 50 nm platinum electrode metal using electron-beam evaporation techniques. These were then patterned using lithographic masking and etching techniques to prevent the exposure of the electrode around the perimeter of the final diced device. 500 nm of stoichiometric silicon nitride was deposited using low-pressure chemical vapour deposition to provide the top insulator. Again using lithography and etching techniques, openings in the top insulation layer were created to define the microelectrodes and contact pads. By varying the used photomasks, both single and arrays of microdisc electrodes were fabricated. A cross-section of a microdisc electrode fabricated by this process is show in Figure 3a. The electrode sizes and pitches of the used arrays is indicated in the figure legends.

This project has received funding from the EURATOM research and training programme 2014-2018 under grant agreement No 755171. The content of this deliverable reflects only the author's view. The European Commission is not responsible for any use that may be made of the information it contains.

Further to these bare platinum electrodes, devices with a coating of Nafion, the ion selective membrane, were made. The structure of the Nafion molecule and a cross-section of the formed film showing the pores in their hydrated state are shown in Figure 4. Nafion was first spin coated at wafer level (after surface modification of the silicon nitride to a silicon oxynitride interface and the use of a silane-based adhesion promoter) and then annealed. Lithographical patterning and plasma etching were then used to remove the Nafion film from the edges of the device and the contact pad. A cross-section of a resulting coated microdisc electrode device is shown in Figure 3b. All electrodes used for the collection of data presented in this report have a Nafion layer thickness of 504 nm at 40 % RH, as measured by profilometry.

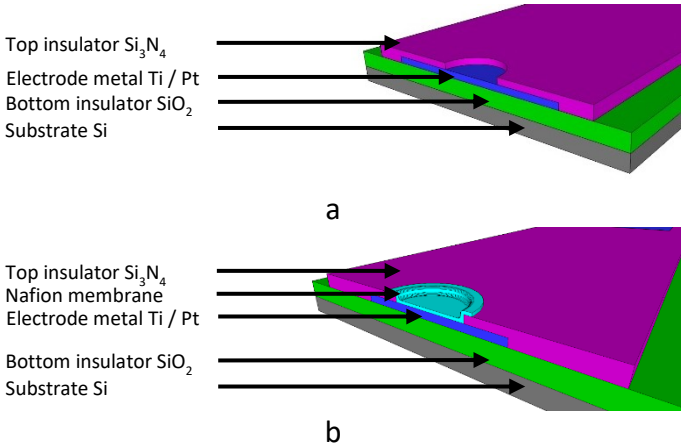

Figure 3 Sketches of (a) a microelectrode and (b) a microelectrode with Nafion coating, a surface functionalising membrane.

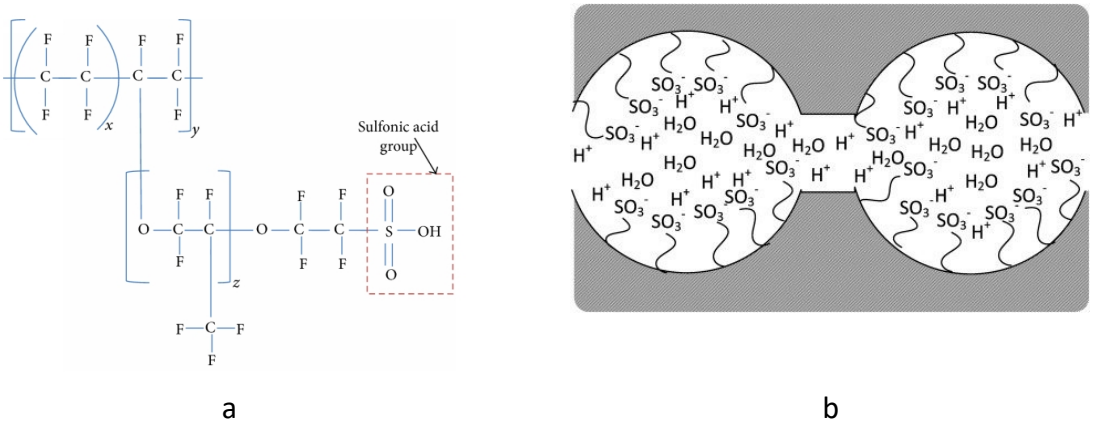

Figure 4 (a) The structure of Nafion the ionomer chosen to be used as a polymer surface film[5] and (b) sketch of the pores and linking channel with their negatively charged sidewalls as formed in the Nafion film[6].

5 Junoh et al., Journal of Nanomaterials, Vol 2015 690965

6 Paridar et al., Electrochimica Acta, 209 (2016) 737-756

This project has received funding from the EURATOM research and training programme 2014-2018 under grant agreement No 755171. The content of this deliverable reflects only the author's view. The European Commission is not responsible for any use that may be made of the information it contains.

MATERIAL COMPATIBILITY

For an optical measurement system, the sensor does not need to be in direct contact with the sample solution, requiring instead an optical window to it. The design of this window presents a design challenge, whilst for an electrochemical measurement, the challenge is that the electrode needs to be in contact with the sample solution and electrically connected to the measuring equipment. This means all used materials for the sensors and connections have to be resilient to the harsh environments they are exposed to. Table 3 presents an overview of material compatibilities with concentrated aqueous nitric acid. Going by this summary (which combines literature knowledge with previous benchmarking experience and proof-of-principle measurements gained during the SACSESS program), the chosen materials and equipment were considered likely to be suitable for experimentation with the relevant analytes extending the capability into array based sensing and to establish longevity.

Table 3 Compatibility of used materials for sensors and measurements setup with nitric acid[7]

Material	**Resistance to nitric acid**	
silicon	yes	forms a very thin protective silicon dioxide surface film
silicon nitride	yes	very low removal rate in hot 60% HNO_3
silicon dioxide	yes	
titanium	yes	corrosion rate of approximately 1mm/year for exposure to boiling 90% HNO_3
platinum	yes	
gold	yes	
Pyrex	yes	
glass	yes	prolonged exposure to boiling, concentrated HNO_3 can cause surface roughening

In addition to the compatibility with nitric acid, the sensors were tested before and after exposure to radiation as an initial attempt to assess radiation compatibility. Platinum microelectrodes, a silver / silver chloride reference electrode and a platinum macroelectrode (with a Nafion coating on a silicon substrate with silicon dioxide and nitride insulators and titanium adhesion layers) were tested both prior to and after irradiation using a 6 MeV γ-ray LINAC source. The sensors were exposed to a total dose of 4 × 6 Gy while sitting in a flat dish filled with 15 mm of phosphate buffered saline to allow for ionisation build up. Electrochemical testing of these devices showed no statistical difference in performance before and after irradiation on all three electrodes (Figure 5). While this is not the most

7 Jang et al., Journal of Vacuum Science & Technology A 19, 267 (2001), Timet: corrosion resistance of titanium (1997)

This project has received funding from the EURATOM research and training programme 2014-2018 under grant agreement No 755171. The content of this deliverable reflects only the author's view. The European Commission is not responsible for any use that may be made of the information it contains.

relevant radiation test for the proposed nuclear application, particularly in terms of dose level, these initial results are nevertheless encouraging and provide the motivation for further active testing. It is therefore concluded that the chosen materials are compatible with the nitric acid and this initial and available radiation environment.

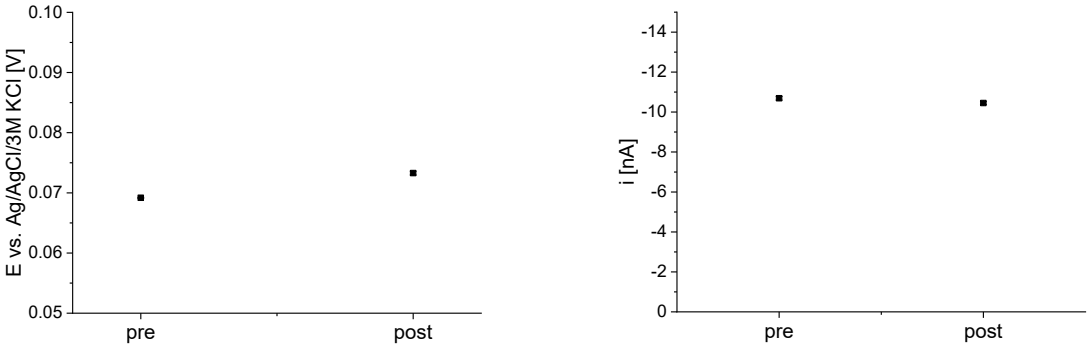

a b

Figure 5 (a) Potential of the on-chip reference electrode vs. a commercial reference electrode and (b) dissolved oxygen reduction current of a 50 µm diameter microdisc electrode before and after irradiation. Error bars are to three standard deviations.

CHEMISTRY

BACKGROUND ON ELECTROCHEMICAL SENSING IN NITRIC ACID WITH MICROELECTRODES

Previous work under the predecessor project SACSESS has established that platinum microelectrodes can be used for electrochemical sensing in the aqueous nitric acid phase. These electrodes were tested in nitric acid of molarities between 0.1 M and 3 M, measuring the components of the nitric acid system, such as nitrite redox reaction (Figure 6a and b), as well as soluble – soluble and soluble – solid redox couples (Figure 6c and d). The work now reported here builds on this SACSESS data.

This project has received funding from the EURATOM research and training programme 2014-2018 under grant agreement No 755171. The content of this deliverable reflects only the author's view. The European Commission is not responsible for any use that may be made of the information it contains.

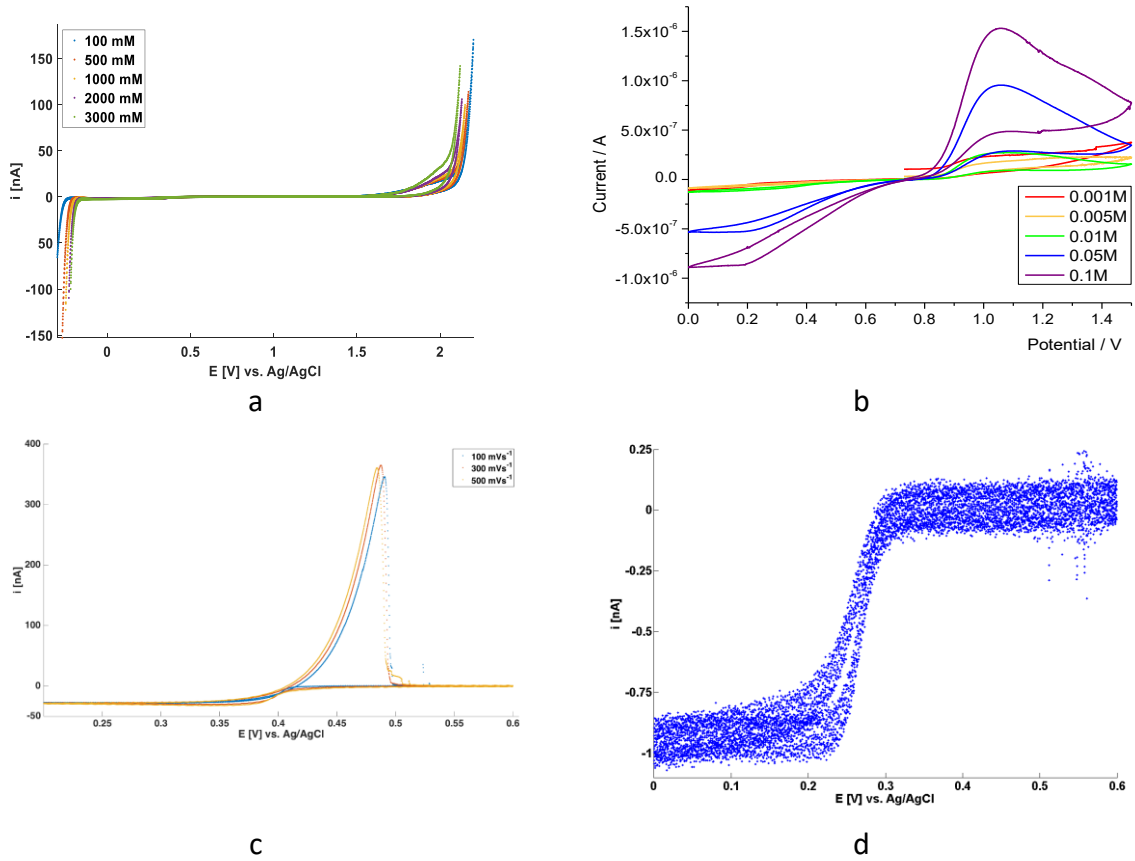

Figure 6 Cyclic voltammograms previously measured and reported in SACSESS of (a) nitric acid of concentrations between 100 mM and 3 M, (b) the nitric - nitrous acid system, (c) silver plating and stripping from silver nitrate in 3 M nitric acid, (d) methylene blue reduction in 0.25 M nitric acid.

HNO_3 SYSTEM WITH AND WITHOUT DEGASSING ON BARE MICRO ARRAY AND NAFION MICRO ARRAY

As previously detailed, nitric acid and its decomposition products potentially undergoes several electrochemical reactions in the potential window of interest. For a single platinum microdisc electrode, and this has been investigated during the SACSESS program as shown above. Figure 7 and 8 show comparison cyclic voltammetry scans of nitric acid using a bare and a Nafion coated microdisc array electrode respectively at a range of scan rates. As expected, both types of array electrodes show significantly enhanced current compared to the previous single microelectrode studies (Figure 6), confirming that an amplified response from the combination of these electrodes was being observed, consistent with the expected enhanced sensitivity. When comparing the coated and uncoated array electrodes, the Nafion coating had consistently slightly reduced measured currents due to the reaction of nitric acid, its associated species and its degradation products, particularly at the faster scan rates, where diffusion kinetics through the pores becomes more significant. The oxygen reduction wave also shows a slight shift to a less positive reduction potential (from 270 mV to 230 mV),

This project has received funding from the EURATOM research and training programme 2014-2018 under grant agreement No 755171. The content of this deliverable reflects only the author's view. The European Commission is not responsible for any use that may be made of the information it contains.

indicating enhanced oxygen gas and/or hydrogen ion activity in the Nafion film, while the hydrogen ion reduction and hydrogen adsorption peaks at E below 0 V are less distinct visible. Together, this suggests a well-coated electrode with no breaks in the polymer film. Interestingly, there is no apparent shift in pH evident in the hydrogen gas generation or oxidation potentials. A pH shift would be expected due to increased proton activity in the film (if there were accumulation of H^+ ions in the channels as a result of a negative Donnan potential induced by a high concentration of fixed negative charges as a result of the polymer backbone anions (Figure 4b). This lack of Donnan potential is likely the result of the relatively large ionic strength of the nitric acid in the solution, and suggests that the shift of the oxygen wave is due to enhanced oxygen activity in the film.

Nafion films were examined prior to and after experimentation to assess their resistance to the environment and the electrochemical testing. Reassuringly, no delamination or optical changes in film structure were found after up to four days of measurements recorded in 500 mM HNO_3(aq).

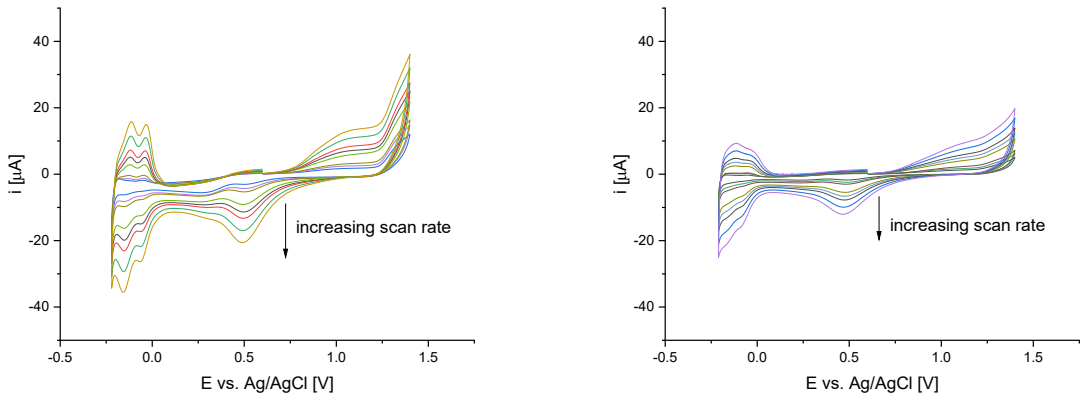

Figure 7 Cyclic voltammograms of 0.5 M HNO_3 recorded at a range of scan rates between 0.1 Vs^{-1} and 0.5 Vs^{-1} on (a) bare and (b) Nafion-coated microdisc arrays with a radius of 25 µm and pitch of 50 µm in a hexagonally closed packed arrangement.

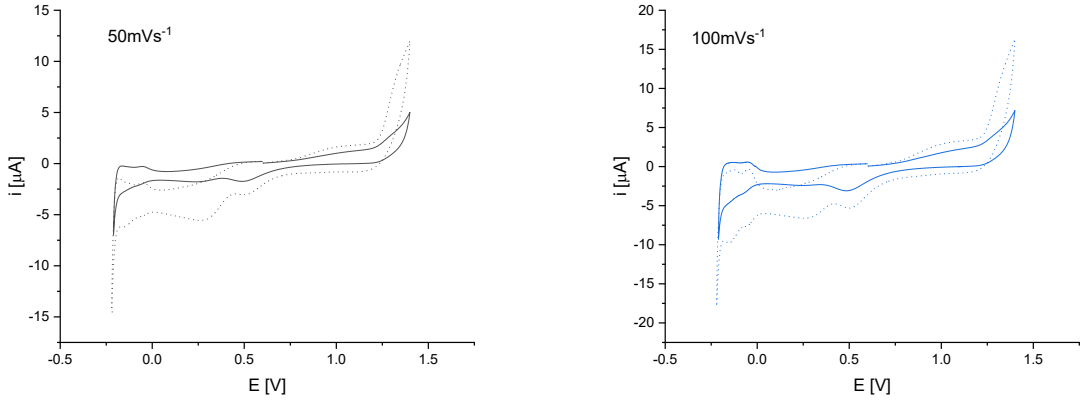

This project has received funding from the EURATOM research and training programme 2014-2018 under grant agreement No 755171. The content of this deliverable reflects only the author's view. The European Commission is not responsible for any use that may be made of the information it contains.

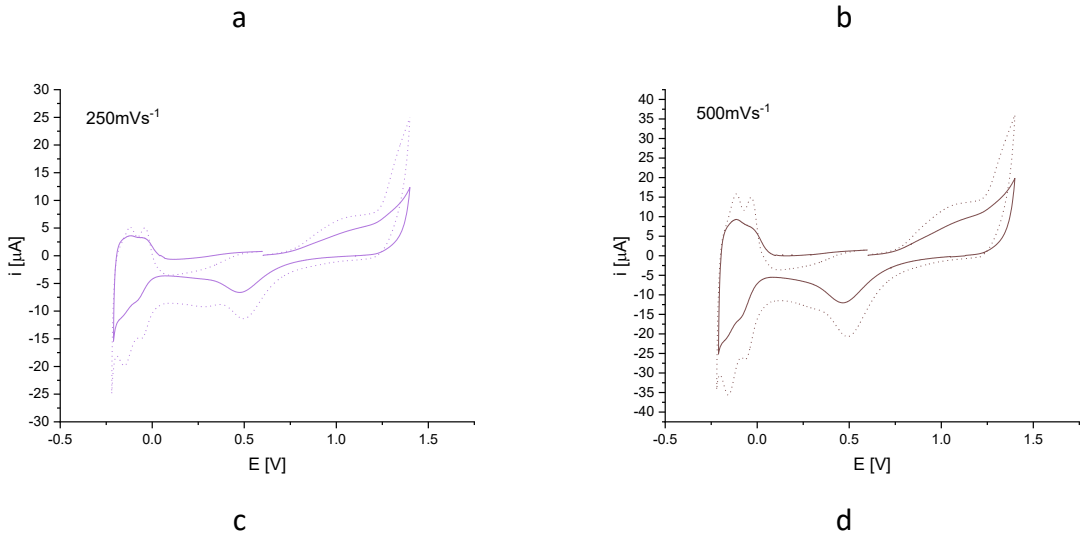

Figure 8 Comparison of selected cyclic voltammograms presented in Figure 7 in aqueous 500 mM HNO_3 solution recorded on bare (dashed) and Nafion-coated (solid) microdisc arrays at (a) 50 mV^{-1}, (b) 100 mV^{-1}, (c) 250 mV^{-1}, (d) 500 mV^{-1}.

EXEMPLAR REDOX COUPLE MEASUREMENTS: FE(III)/FE(II)

Fe^{III} is used as an exemplar metal ion to test the capabilities in quantitative monitoring of these sensor systems. Iron is a common corrosion product of steel and will therefore likely be present in the process. Quantitation and the presence of iron will therefore be an indicator of the corrosion degree and state of steel used e.g. for piping and vessels in the system. In addition to that, Fe^{III} will potentially be partially co-extracted as a contaminant. Figure 9 and Figure 10 show cyclic voltammetry and differential pulse voltammetry scans (CV, DPV) of the reduction of Fe^{III} to Fe^{II} in 500 mM HNO_3. The data show the expected microelectrode response; a reduction wave leading to a steady state mass transport limited current for the CV and a near-symmetrical peak for the DPV. This allows the ready monitoring of Fe through the $Fe^{III/II}$ redox reaction.

It is clear that the mass transfer limited currents in these experiments are at very low levels of around 1 nA for CV and 0.1 nA for DPV when using these single disc electrodes, even at this relatively high concentration of 1 mM. There is already some noise in the DPV response and this level is likely to become problematic when analysing smaller currents resulting from the complexation of a fraction of the ions to organic ligands and/or due to a smaller overall concentration. A simple way to increase the observed current without changing the microelectrode size is to use multiple microelectrodes in an array, as the multiple microdisc electrodes are in parallel and result in a multiplication of the overall current by the number of electrodes in the array (as discussed in choice of electrodes above). All data shown subsequently were therefore recorded on array devices.

This project has received funding from the EURATOM research and training programme 2014-2018 under grant agreement No 755171. The content of this deliverable reflects only the author's view. The European Commission is not responsible for any use that may be made of the information it contains.

In addition to employing bare platinum microdisc arrays, the response of microelectrode arrays coated with Nafion surface films was measured. As has been discussed above, the use of these surface films, which selectively exclude or favour specific electroactive components, should allow the easier differentiation of signal components and thus facilitate analysis. The Nafion coating, which is a hydrated surface polymer film consisting of a Teflon backbone terminated with negatively charged sulphonate groups within nanochannels and micrometre range diameter pores, was developed for fuel cells and is therefore stable in strong acid.

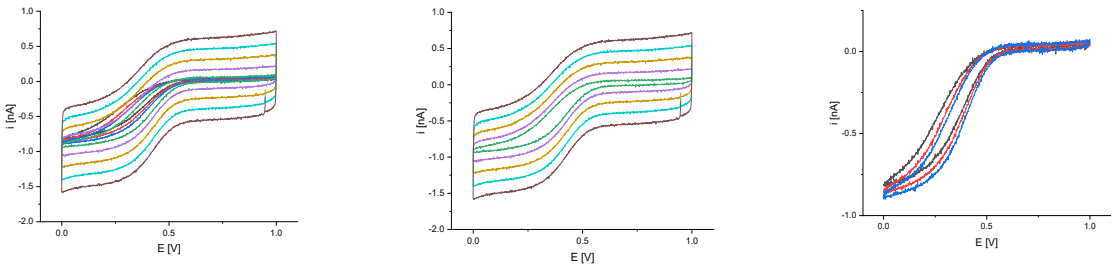

a b c

Figure 9 Cyclic voltammograms of 1 mM Fe^{III} nitrate in 500 mM aqueous HNO_3 recorded on a 10 µm diameter platinum microdisc electrode at scan rates of (a) 25, 50, 75, 100, 200, 300, 400, 500 mVs^{-1}, (b) 100, 200, 300, 400, 500 mVs^{-1} (c) 25, 50, 75 mVs^{-1}.

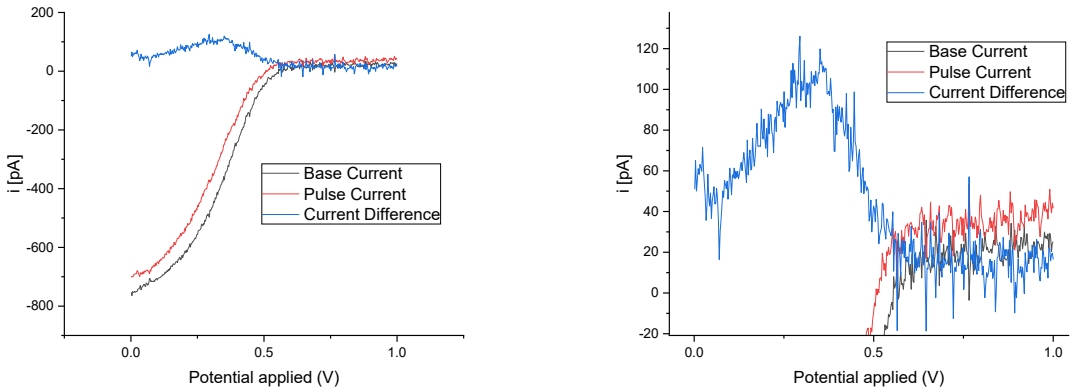

a b

Figure 10 (a) differential pulse voltammograms of 1 mM Fe^{III} in 500mM HNO_3 recorded on a platinum microdisc electrode. (b) shows a magnification of the data presented in (a).

Figure 11 and Figure 12 show CVs at a range of scan rates for both a bare platinum and a Nafion coated platinum microelectrode array system. (In these array systems the microelectrode array has been designed to be closely spaced so as to maximise currents and will be expected produce a macroelectrode like response at these scan rates due to the promotion of the overlap of neighbouring diffusion fields and the establishment of linear diffusion across the array). This is confirmed by the bare response (Figure 11a), in which the expected $Fe^{III/II}$ redox peak currents are present, which also show the expected dependency on the square root of the scan rate at the slower scan rates, indicating planar diffusional control.

This project has received funding from the EURATOM research and training programme 2014-2018 under grant agreement No 755171. The content of this deliverable reflects only the author's view. The European Commission is not responsible for any use that may be made of the information it contains.

When looking at the Nafion-coated electrode array response (Figure 11b), it is clear that the $Fe^{III/II}$ reduction occurs at close to the same reduction potential as on the uncoated array and the onset of the reduction current is very similar for both arrays, which is consistent with lack of a Donnan potential. However, the Nafion-coated electrode array exhibits a sharper and higher first peak current which then reduces to the same current as the bare array at the negative vertex potential. This extra current measured and the sharpness of this additional peak in the first scan is likely caused by an excess accumulation of Fe^{III} ions in the Nafion film pores prior to CV cycling due to the thermodynamically favourable multiple electrostatic binding of the Fe^{III} with several negatively charged sulphonate groups on the sidewalls. The very small change in re-oxidation current observed on bare and Nafion coated electrodes at each scan rate (Figure 12) suggests that this additional Fe^{III} is reduced and rapidly expelled during the first reductive scan and does not contribute to the oxidation peak current.

This makes the Nafion coating very useful for an online monitoring sensor. The coating reliably simplifies the nitric acid redox response while enabling the non-complexed Fe^{III} to pass through the film not only without current dampening or a shift in reduction current but also through increasing the initial current observed by prior enhancement of the number of Fe^{III} cations in the membrane. This offers the prospect of sensitive redox cation monitoring and discrimination through size of non-complexed cations such as Fe^{III}.

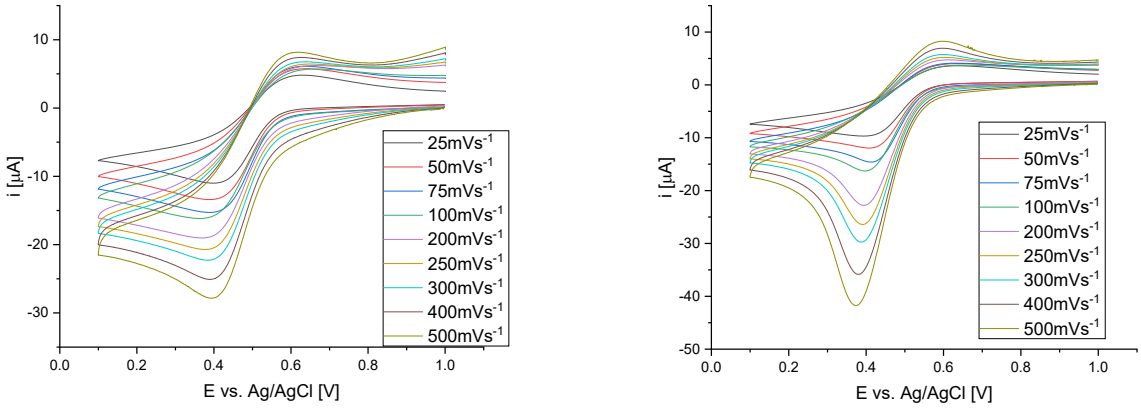

Figure 11 Typical first scan cyclic voltammograms of 1.5 mM Fe^{III} nitrate in 500 mM HNO_3 recorded on (a) an uncoated and (b) a Nafion-coated microdisc array with a radius of 25 µm and pitch of 50 µm in a hexagonally closed packed arrangement at the scan rates indicated in the legend.

This project has received funding from the EURATOM research and training programme 2014-2018 under grant agreement No 755171. The content of this deliverable reflects only the author's view. The European Commission is not responsible for any use that may be made of the information it contains.

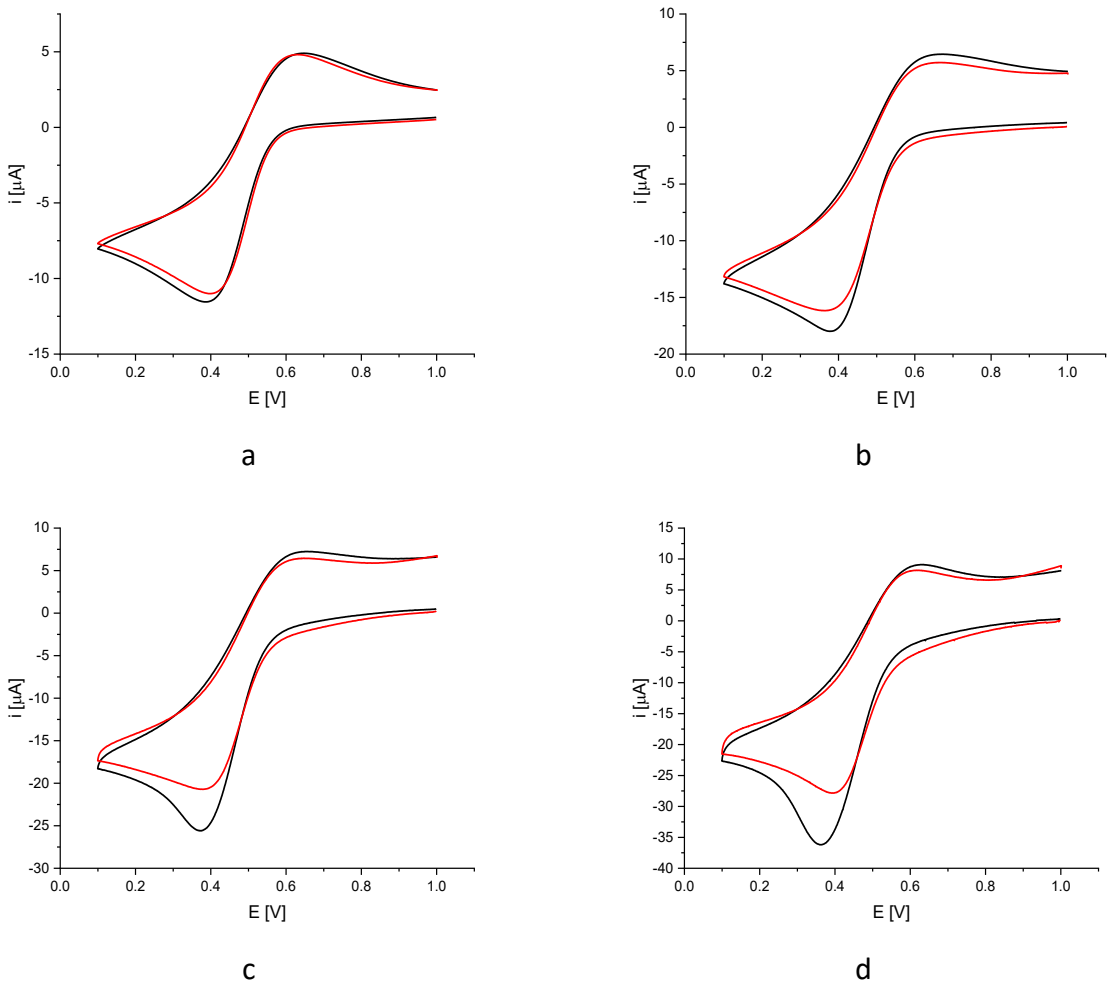

Figure 12 Direct comparison of the first scan cyclic voltammograms of 1.5 mM Fe^{III} in 500 mM HNO_3 recorded on an uncoated (red) and Nafion-coated (black) microdisc at scan rates of (a) 25 mV^{-1} , (b) 100 mV^{-1}, (c) 250 mV^{-1} and (d) 500 mV^{-1}.

At lower Fe^{III} concentrations, the contribution to the current of the coincident oxygen reduction wave was found to become progressively more important. Therefore, degassing through sparging with argon was utilised henceforth to remove this additional contribution to the current.

Figure 13 shows CVs of the serial addition of Fe^{III} to aqueous sparged 500 mM nitric acid over the potential window relevant for the monitoring of the iron reduction reaction. While the additional Fe^{III} reduction current is now visible as a progressive increase in the reduction current below +0.4 V with increasing concentration against the constant nitric acid electrochemistry the CV method is not ideal for quantification, especially due to the significant overlapping nitrite reduction peak at approximately 0.45 V.

In contrast Figure 14a and b therefore show corresponding differential pulse voltammetry (DPV) scans which shows the significantly clearer Fe^{III} reduction peak produced by this

This project has received funding from the EURATOM research and training programme 2014-2018 under grant agreement No 755171. The content of this deliverable reflects only the author's view. The European Commission is not responsible for any use that may be made of the information it contains.

technique, with a peak current of constant potential (Figure 14c) which is seen to increase linearly with concentration and give a negligible background current (Figure 14d). Compared to the CV, the DPV technique is less affected by charging and background currents which explains its increased sensitivity to Faradaic currents. It is also noteworthy that the Gaussian peak analysis is much simpler than that required for the CV.

As the Fe^{III} addition leads to a smoothly and linearly increasing DPV peak height at a close to constant reduction potential / peak position (Figure 14c and d), for the purpose of concentration monitoring in nitric acid, DPV is therefore considered the most suitable technique.

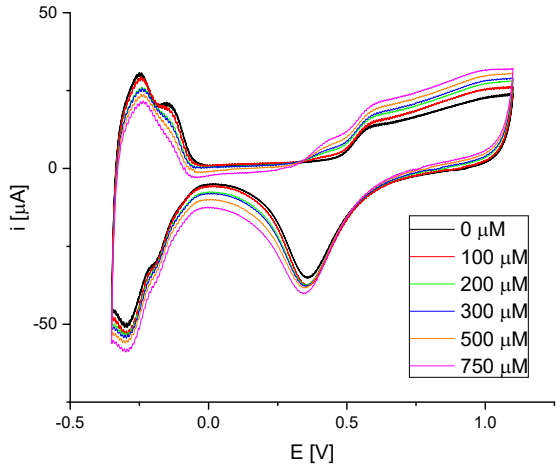

Figure 13 CV of serial addition of Fe^{III} into 500 mM HNO_3 recorded on a microdisc array with a radius of 15 µm and pitch of 25 µm in a hexagonally closed packed arrangement at 500 mVs^{-1}.

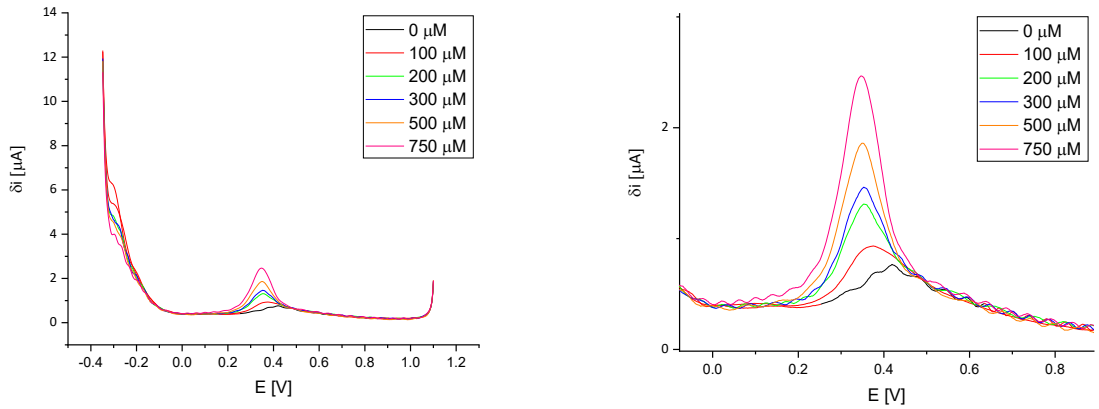

This project has received funding from the EURATOM research and training programme 2014-2018 under grant agreement No 755171. The content of this deliverable reflects only the author's view. The European Commission is not responsible for any use that may be made of the information it contains.

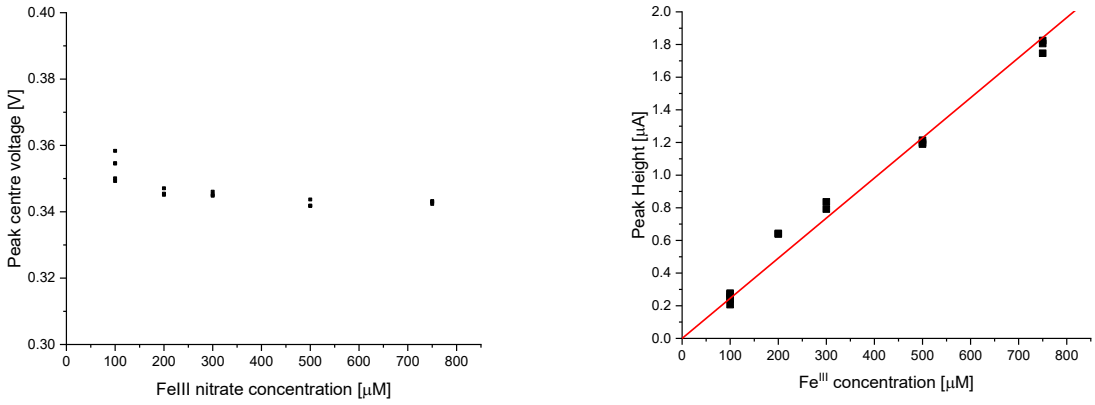

c d

Figure 14 (a) DPV of serial addition of Fe^{III} into 500 mM HNO_3 recorded on a microdisc array with a radius of 15 µm and pitch of 25 µm in a hexagonally closed packed arrangement. (b) is a magnification of the data presented in (a). (c) and (d) are extracted values for peak position and height extracted via Gaussian fitting.

EXEMPLAR REDOX COUPLE MEASUREMENTS: CE(III)/CE(IV)

Cerium is of interest as an analogue for plutonium. Electrochemically, it is an interesting candidate for monitoring as it potentially undergoes a $Ce^{III/IV}$ reaction at the upper end of the potential window at these pHs (Table 2). Figure 15a therefore shows typical CV scans of this reaction on a bare platinum array which clearly show the expected additional oxidation wave at approximately 1.5 V. While studying this reaction is clearly of interest, the initially formed Ce^{IV} is by definition a highly oxidising ion, and thermodynamically it would spontaneously react chemically to form solid CeO_2 (Table 2). Consistent with this, a white solid was observed to form and also (consistent with the oxidising power of Ce^{IV}) prolonged oxidation was observed to lead to removal of the bare platinum microelectrodes. This is unsurprising, as nitric acid and Ce^{IV} are the main components of a commonly used etching solution for a range of transition metals.[8] It is interesting therefore that in this initial study, the Nafion coated electrode was observed to hinder the Ce^{III} oxidation and prevent platinum dissolution (Figure 15b) across a continuous 24 hour long measurement, a time frame that was sufficient to fully remove the platinum exposed to the solution on an uncoated device. This suggest that the Nafion film is protecting the underlying electrode by suppressing Ce^{IV} formation and preventing attack of the underlying platinum electrode, and may produce the same effect when producing other highly oxidising ions.

[8] Nichrome Etchants TFN, Transene Company, Inc. (10 – 20 % $(NH_4)_2Ce(NO)_6$ + 5 – 6 % HNO_3 + H_2O)

This project has received funding from the EURATOM research and training programme 2014-2018 under grant agreement No 755171. The content of this deliverable reflects only the author's view. The European Commission is not responsible for any use that may be made of the information it contains.

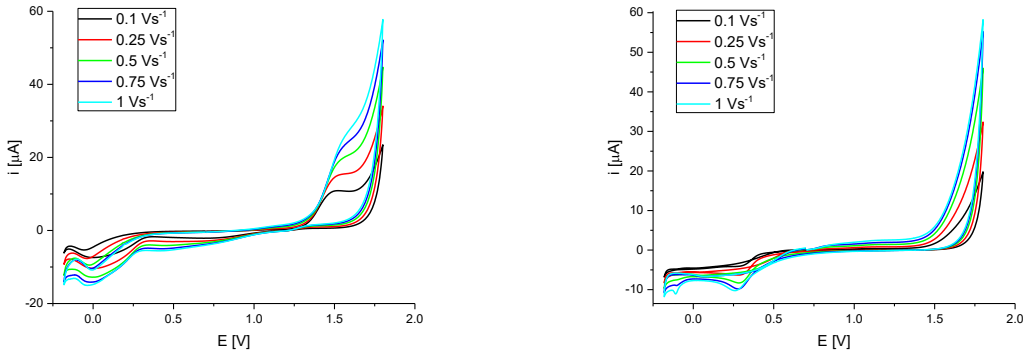

Figure 15 Cyclic voltammograms recorded on (a) a bare and (b) a Nafion coated Pt microelectrode array in 1 M HNO_3 / 2 M KNO_3 with 1 mM $Ce(NO_3)_3$. The microarray has a radius of 25 µm and pitch of 75 µm in a hexagonally closed packed arrangement.

EXEMPLAR STUDY OF COMPLEXATION OF FE(III) WITH SO_3-PH-BTBP

UREAD has supplied us with 2,6-Bis(5,6-(di(sulfophenyl)-1,2,4-triazin-3-yl)-1,4-bipyridine (SO_3-Ph-BTBP, Figure 16), a model hydrophilic extractant that with TODGA has been shown to be a promising candidate for the extraction of Am^{III} from Cm^{III} and Ln^{III}.[9] Here it is used to study differences in electrochemical signature between free and complexed metal ion, in this case Fe^{III} on the microelectrode arrays, to assess the potential for complexation monitoring.

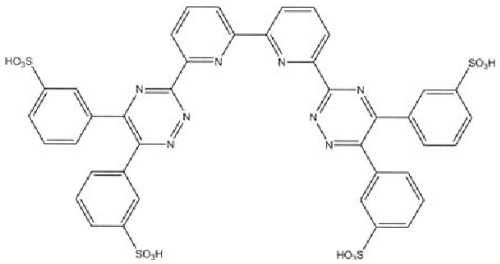

Figure 16 Structure of SO_3-Ph-BTBP hydrophilic ligand

As optical spectroscopy is the main alternative to electrochemistry for online monitoring of the solvent extraction process. UV/vis and fluorescence spectroscopy data are presented here to offer a benchmarking comparison for the chosen exemplar complexation of Fe^{III} with SO_3-Ph-BTBP. Figure 17 shows the UV/vis spectra of non-complexed 100 µM SO_3-Ph-BTBP and after addition of 100 µM Fe^{III}. SO_3-Ph-BTBP has a sharp absorbance peak at approximately 320 nm. Upon Fe^{III} addition, only a small change in absorbance is apparent at around 400 nm, with no characteristic shift in position or intensity of the main SO_3-Ph-BTBP peak.

[9] Wagner et al. *Solvent Extraction and Ion Exchange*, 2016, 34 (2), 103-113

This project has received funding from the EURATOM research and training programme 2014-2018 under grant agreement No 755171. The content of this deliverable reflects only the author's view. The European Commission is not responsible for any use that may be made of the information it contains.

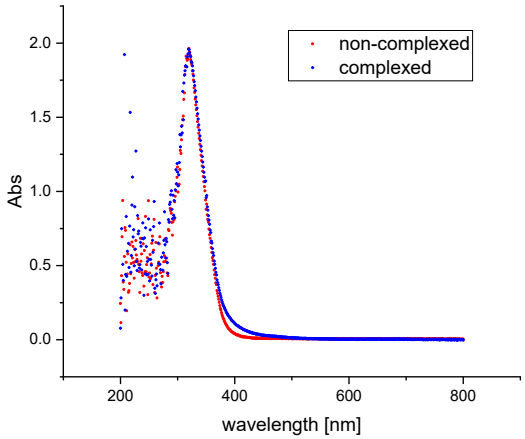

Figure 17 UV/vis spectrum of 100 µM SO_3-Ph-BTBP in 500 mM HNO_3 prior to and following the addition of 100 µM Fe^{III}.

By contrast Figure 18a shows fluorescence emission spectra of the SO_3-Ph-BTBP solution alone and with serial additions of Fe^{III} on excitation at 350 nm. SO_3-Ph-BTBP shows a wide emission peak at approximately 440 nm that decreases and shifts to about 480 nm after the addition of the Fe^{III}. Figure 18b shows the dependence of the peak height on the Fe^{III} concentration. Linear fitting to the lowest and highest Fe^{III} concentrations leads to a found intercept between the two regression fits of 101 nM indicating that SO_3-Ph-BTBP and Fe^{III} form a strong solution complex through titration with an ion: ligand stoichiometric ratio of 1:1.

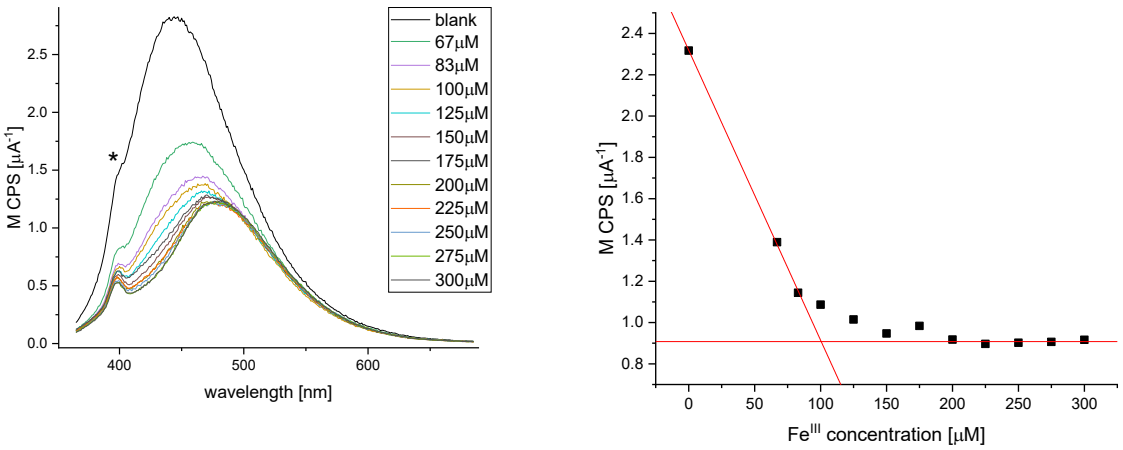

a b

Figure 18 (a) Fluorescence spectroscopy emission spectra of 100 µM SO_3-Ph-BTBP in 500mM HNO_3 with added Fe^{III} (excitation at 350 nm). The additional peak indicated by * is due to Raman scattering. (b) shows the peak heights extracted from (a) using Gaussian fitting as a function of the Fe^{III} concentration.

Figure 19 shows the corresponding baseline DPV scan of 100 µM SO_3-Ph-BTBP in 500 mM HNO_3. It shows two peaks, indicating redox reactions, at ca. 0.09 V (Peak I) and 0.42 V (Peak IV). It is satisfying that Peak IV has previously been found in DPV measurements of 500 mM

This project has received funding from the EURATOM research and training programme 2014-2018 under grant agreement No 755171. The content of this deliverable reflects only the author's view. The European Commission is not responsible for any use that may be made of the information it contains.

nitric acid and the serial addition of Fe^{III} (Figure 14) and was identified as being due to nitrite reduction. As expected from the analysis of this peak as originating from nitric acid species, this peak does not change during the complexation of metal ions with the SO_3-Ph-BTBP. The more negative potential peak (Peak I) is additional and is therefore consistent with a reduction reaction associated with the added SO_3-Ph-BTBP ligand.

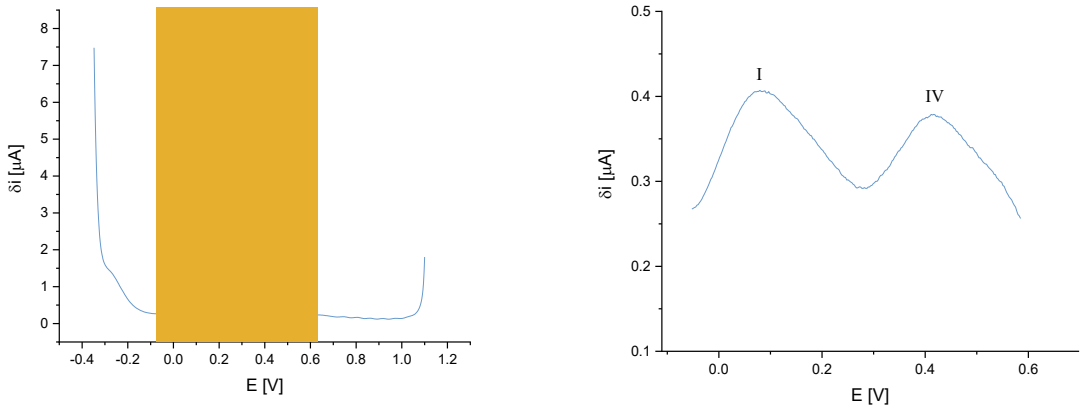

Figure 19 (a) DPV scan of 100 μM SO_3-Ph-BTBP in 500 mM nitric acid recorded on a microdisc array with a radius of 25 μm and pitch of 50 μm in a hexagonally closed packed arrangement. (b) shows a magnification of the region of interest also highlighted in (a).

Figure 20a shows exemplar DPV data for the equivalent experiment to the above fluorescence spectroscopy data; the serial addition of Fe^{III} to 100 μM SO_3-Ph-BTBP in 500 mM nitric acid. Some of the data suffered from electrical noise in the form of a defined sinusoidal wave, visible especially in the data between 0.6 V and 1.0 V. Prior to analysis, the data was therefore FFT filtered. Figure 20b shows the FFT filtered DPV of 100 μM each Fe^{III} and SO_3-Ph-BTBP with the fitted Gaussian peaks. Upon Fe^{III} addition, two peaks grow in. As one (Peak III) is very similar in potential to the $Fe^{III/II}$ reduction peak found in the SO_3-Ph-BTBP-free measurements (Figure 14) at approximately 0.342 V, it is also assigned to Fe^{III}/Fe^{II} reduction. The second peak which also increases in magnitude with added Fe^{III} is close in position to Peak I, which was previously attributed to a reduction involving added SO_3-Ph-BTBP in Figure 19.

Peak fitting of the DPV at all concentrations shows that the data can be fitted successfully to either three or four Gaussian peaks. In three peak fitting, Peak I/II at ~0.1 V is considered as one peak. This peak both increases in magnitude and shifts positive in peak potential with increasing iron concentration. When fitting with four peaks, Peaks I and II appear to have essentially constant potentials. In this case it is assumed that Peak I is due to the SO_3-Ph-BTBP prior to Fe^{III} addition and Peak II is due to the 1:1 Fe^{III}-SO_3-Ph-BTBP complex.

The similarity of the peak position of Peak III to the peak found to correspond to non-complexed $Fe^{III/II}$ (Figure 14) is interesting, since the fluorescence data indicated that all the

This project has received funding from the EURATOM research and training programme 2014-2018 under grant agreement No 755171. The content of this deliverable reflects only the author's view. The European Commission is not responsible for any use that may be made of the information it contains.

added Fe^{III} strongly complexes with the SO_3-Ph-BTBP in a 1:1 complex, which suggests that the complexation does not lead to a significant shift in the $Fe^{III/II}$ reduction potential, and that both Fe^{III} and Fe^{II} are equally strongly complexed. Peak IV is the nitrite reduction also detected in the SO_3-Ph-BTBP-free Fe^{III} measurements (Figure 14) and the Fe^{III}-free SO_3-Ph-BTBP measurements (Figure 19). It is therefore again reassuring that Peak IV is constant throughout the fits in this experiment, as the nitrite concentration would not be expected to vary.

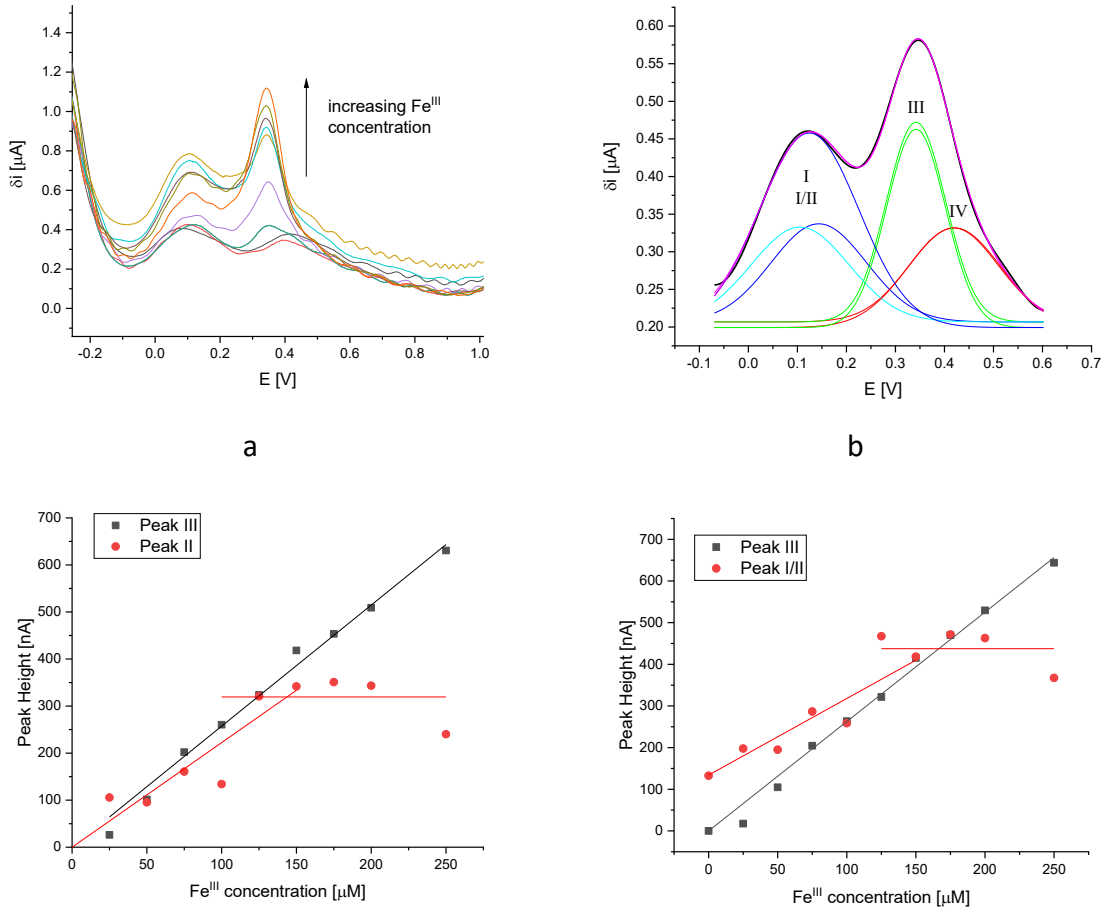

Figure 20 (a) DPV of serial addition of Fe^{III} to 100 μM SO_3-Ph-BTBP in 500 mM nitric acid recorded on a microdisc array with a radius of 25 μm and pitch of 50 μm in a hexagonally closed packed arrangement. (b) shows the FFT filtered DPV of 100 μM each Fe^{III} and μM SO_3-Ph-BTBP and the three or four Gaussian peaks fitted to the response. (c) presents the variation in heights of peaks II and III as a function of Fe^{III} addition. (d) presents the variation in in heights of peaks II and III as a function of Fe^{III} addition assuming peaks I and II are one peak rather than two.

We have previously shown that using electrochemical microelectrodes, the nitrite reduction reaction can be quantitatively measured using CV. We now show that it can also be measured using the DPV technique. Figure 20c and d show the variation of the peaks heights of Peaks II and III (four peak fit) and combined Peak I/II and III (three peak fit) with added iron. Irrespective of which model is chosen, it is satisfying that a linear relationship between Peak

This project has received funding from the EURATOM research and training programme 2014-2018 under grant agreement No 755171. The content of this deliverable reflects only the author's view. The European Commission is not responsible for any use that may be made of the information it contains.

III and Fe^{III} concentration is found in both cases (consistent with Peak III being due to $Fe^{III/II}$ reduction) whilst Peak I/II and Peak II each show a linear relationship with Fe^{III} concentration up to ~100 µM added iron, after which the peak height remains constant within experimental error. Peak II is also of the same magnitude as Peak III below 100 µM added iron within experimental error. Together, this therefore indicates that peak II is diagnostic of a further one electron reduction of the 1:1 complex, which would be consistent with a further reduction of the 1:1 ligand / Fe^{II} complex (most likely accepting an electron into a combined metal-ligand orbital).

The only feature left to explain is the origin of Peak I, the additional reduction peak seen in the ligand solution before Fe^{III} addition. It would be tempting to assign this to the one electron reduction of the non-complexed ligand; however, it is hard to explain why this would only be one quarter of the magnitude of the one electron reduction peaks seen for the 1:1 complex. We therefore tentatively assign this to the reduction of a proportion of the ligand which is already complexed prior to Fe^{III} addition, due to cation impurities present during ligand synthesis and/or due to cation impurities in the nitric acid (the expected concentration of which is lower than but within an order of magnitude of the required 25 µM concentration). We aim to confirm this in subsequent measurements.

CONSIDERATIONS ON INFLUENCING FACTORS ON THE MEASURED SIGNAL

In a reprocessing system, multiple components of the solution are expected to vary over time, presenting a challenge for the identification of analytes varying in both signal magnitude (current) and location (reduction potential). Most of these variations are expected to be gradual (and e.g. potential changes to be smaller than, and predictably related to, current changes) which enables the deconvolution and tracking of signature peaks over time to facilitate their identification, a key enabler of online monitoring. In addition, there are variations between different sensor locations within the flowsheet in terms of the different acidities used, flow and mixing regimes, analytes present and their concentrations which presents highly different starting conditions. Ideally these sensor systems should be able to monitor under all of these conditions; these initial studies do not highlight any showstoppers at this stage, but in establishing applicability, some measurement variations will be more important than others, which will impose a hierarchy of measurement and analysis validation. For example, in subsequent studies, the measurements presented above will be repeated for different nitric acid concentrations to demonstrate the applicability of, and potential for, speciation measurement and monitoring across the acidity range.

In addition, previous work for the SACSESS project has shown the change in signal due to NOx species as a function of nitric acid concentration (Figure 21). All peaks assigned to nitric species

This project has received funding from the EURATOM research and training programme 2014-2018 under grant agreement No 755171. The content of this deliverable reflects only the author's view. The European Commission is not responsible for any use that may be made of the information it contains.

in this study were found to vary smoothly and predictably with nitric acid concentration. Other reactions, such as the silver plating – stripping reaction (Figure 6c) do not depend on acidity or nitric concentration (In general, redox currents will vary with the acid concentration or nitric acid concentration if protons or nitric species are involved in the redox reaction)

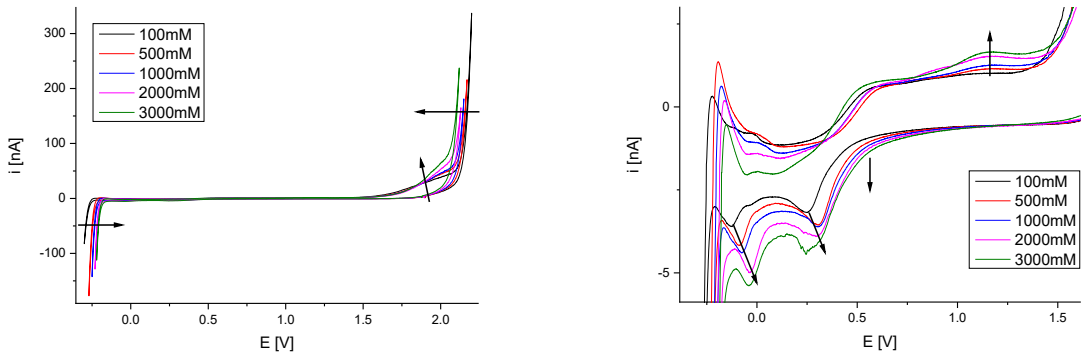

Figure 21 Cyclic voltammograms of nitric acid at varying concentrations with ionic strength adjusted to 3 M using potassium nitrate. Data was recorded on a single platinum microdisc electrode with a radius of 5 µm at a scan rate of 500 mVs^{-1}. The arrows indicate the change in signal with increasing acidity.

For the chosen exemplar redox reaction of Fe^{III} to Fe^{II}, no protons are involved in this reaction under acidic conditions. As for $Ag^{I/0}$, no pH dependence is therefore expected for this reaction within the concentration range considered for the extraction process. However, some reactions that can be monitored electrochemically do involve protons (see Table 2); the potential and nature of these reactions should therefore be affected in a predictable manner by the varying pH, which can be stablished and is likely to aid in signal detection and deconvolution. Other factors may also lead to measureable, reproducible and characteristic changes in electrochemical signature for species monitoring. For example, redox reactions and/or complexation between nitric and metal ion species may lead to the reduction and corresponding growth in the signal for redox reagents and products.

This proof or principle work has therefore highlighted the real potential of electrochemical measurement, analysis and deconvolution of the response of selected and representative mixtures using these electrode systems, to first characterise and then demonstrate the potential to monitor such factors as redox state, composition (nature and amount of species), acidity and speciation. It is also worth considering the challenges and opportunities of such deconvolution in complex multianalyte system such as those seen in extraction for nuclear reprocessing. Previous theoretical work during SACSESS has shown a minimum difference in reduction potential of 10 mV at room temperature in DPV to enable the deconvolution of the response of two electrochemically reversible redox reactions with equal peak current magnitude. Although this separation requirement was shown to become slightly larger as the peak heights became more unequal, given the potential scan range of 1-2 Volts, this offers the

This project has received funding from the EURATOM research and training programme 2014-2018 under grant agreement No 755171. The content of this deliverable reflects only the author's view. The European Commission is not responsible for any use that may be made of the information it contains.

prospect of complex multicomponent (multipeak) detection, deconvolution and discrimination of a large number of redox-active species.

SUMMARY, CONCLUSIONS AND WAY FORWARD

The results presented in this deliverable report together indicate that we have developed electrochemical microelectrode array sensor systems which are capable of electrochemical measurements rich in diagnostic information, specifically enabling quantitative electrochemical analysis in the harsh environment presented by the acid systems required for EURO-GANEX liquid-liquid extraction, and which are unaffected by initial irradiation tests. The enhanced electrochemical pulse technique of Differential Pulse Voltammetry, has shown superior performance in terms of enhanced sensitivity, decreased background and increased signal-to-noise compared to the more commonly used cyclic voltammetry. Nafion has also been shown to be an effective, acid stable, protective and selectively permeable polymer membrane for the protection of the platinum from corrosive ion formation such as Ce^{IV}. It is also capable of screening out large ions and/or molecules due to its characteristic pore size in the range of single nanometres. This opens up the prospect of selective detection of free cations without detection of bulky iron complexes. The backbone anions of these pores additionally make it potentially able to favour cation (Fe^{III}) aggregation through selective binding.

In terms of quantitative detection, analysis of the DPV response on bare platinum arrays has indicated quantitative electrochemical reduction peaks characteristic of nitrite, a 1:1 Fe^{III}-ligand complex and total Fe^{III} for the exemplar Fe^{III} and ligand (SO_3-Ph-BTBP) system. These measurements are consistent with benchmark fluorescence measurements but richer in information, in providing independent measurement of total Fe^{III} present in solution, complexed Fe^{III} and nitrite concentration. That the SO_3-Ph-BTBP:Fe^{II} complex apparently undergoes a further one electron electrochemical reduction (most likely involving mixed metal ligand orbitals) potentially opens up the possibility of detecting other metal ions that do not undergo an electrochemical redox reaction when uncomplexed, either through a similar complex reduction or through the addition of conjugated redox active groups to the ligand to report on metal complexation. When combined with the established microelectrode array characteristics of enhanced detection sensitivity, lower susceptibility to convection and lower limits of detection, these proof of principle results demonstrate the potential of these systems for process characterisation and for sensing and monitoring and underscore the potential for equivalent measurements on, and monitoring of, other metal ion relevant species in Table 2.

This project has received funding from the EURATOM research and training programme 2014-2018 under grant agreement No 755171. The content of this deliverable reflects only the author's view. The European Commission is not responsible for any use that may be made of the information it contains.

In addition, since the start of the GENIORS project, we have successfully applied for a follow up grant from the UK's Engineering and Physical Sciences Research Council (EPSRC) as part of the Accident Tolerant Fuels in Recycle (ATLANTIC) programme to investigate extraction monitoring in flowing systems. This program will commence following the completion of the GENIORS grant and will be used as leveraged funding to examine and establish applicability to extraction in a mixed flow system. Selected results from these studies will be presented to the GENIORS community through future HYPARs. Schematic diagrams of some of the system to be used for this work are shown in Figure 22.

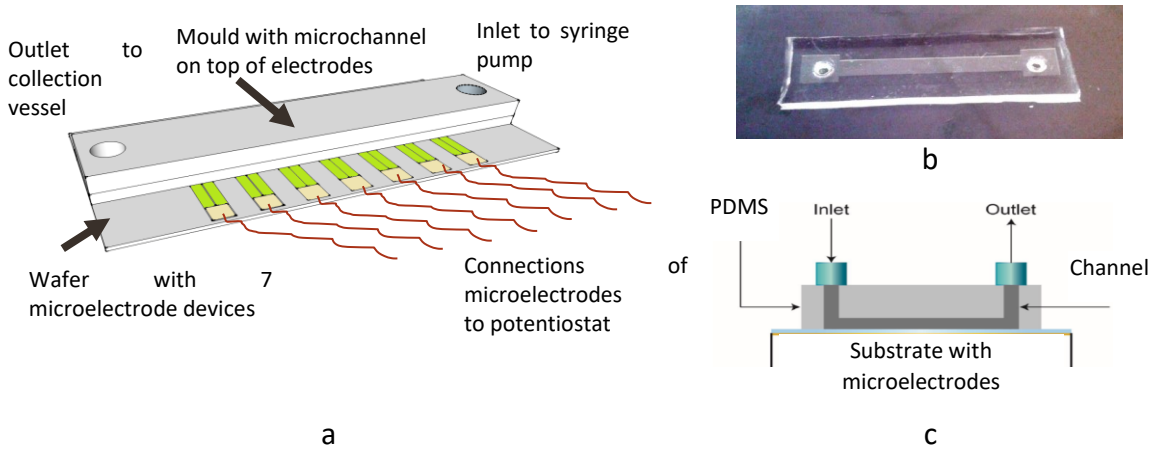

Figure 22 Designed setup for measurements under flow conditions. (a) A 3D sketch of the microelectrode with bonded PDMS microchannel. (b) A photograph of a PDMS microchannel prior to bonding to the silicon substrate. (c) A cross-section of the setup.

ANNEXES

MATERIALS

All used chemicals are of analytical grade. SO_3-Ph-BTBP was supplied by our collaborator UREAD as part of their contribution to GENIORS.

This project has received funding from the EURATOM research and training programme 2014-2018 under grant agreement No 755171. The content of this deliverable reflects only the author's view. The European Commission is not responsible for any use that may be made of the information it contains.